Widely Tunable Negative-Chirp SG-DBR Laser/EA-Modulated Transmitter

J. W. Raring, *Student Member, IEEE*, E. J. Skogen, *Member, IEEE*, L. A. Johansson, *Member, IEEE*, M. N. Sysak, *Student Member, IEEE*, S. P. DenBaars, *Member, IEEE*, and L. A. Coldren, *Fellow, IEEE*

***Abstract*—Ten Gb/s low power penalty (< 0.5 dB) error-free transmission was achieved through 75 km using a high-performance sampled-grating (SG) distributed Bragg reflector (DBR) laser/EAM transmitter. Large signal chirp measurements show negative chirp operation across the entire tuning range of the devices. An integration-oriented quantum-well-intermixing (QWI) process was employed for the realization of these devices.**

***Index Terms*—Chirp, electroabsorption modulators (EAMs), ion implantation, laser tuning, optical fiber communication, quantum-well intermixing (QWI), semiconductor lasers, wavelength division multiplexing (WDM).**

I. Introduction

ELECTROABSORPTION-MODULATED widely tunable transmitters are candidate sources for optical metropolitan area network applications, as they are compact and potentially low cost. The monolithic integration of electroabsorption modulators (EAM) with widely tunable lasers allows for inventory reduction and wavelength agile functionality. A common method used to realize this integration employs an offset quantum-well (QW) epitaxial architecture, in which the QW active region is grown on top of a bulk waveguide. For EAM definition, the QWs are selectively etched away and an upper cladding regrowth is performed [1]. This process produces Franz-Keldysh type modulators with a positive chirp factor, not suitable for 10 Gb/s transmission through standard fiber over distances required in metro networks. If QWs are used in the EAM, the quantum-confined stark effect can be exploited, and negative chirp factors can be achieved. Power-penalty-free transmission through over 100 km of standard fiber using QW EAMs has been reported [2]. The traditional method for the realization of monolithically integrated diode laser/QW-EAM transmitter involves the selective removal of the as-grown waveguide/multiple QW (MQW) region followed by the regrowth of waveguide/MQW material with the desired band edge. This tedious method is commonly referred to as butt-joint regrowth [3]. Although the butt-joint regrowth process does allow each integrated component to possess a unique band edge, the difficulty associated with matching thickness and achieving the desired composition to avoid reflection and loss at the interface is great. Another technique used to realize multiple band edges across a wafer is selective area growth. However, as discussed in [4] the abruptness of the transition region is limited by the surface diffusion of the growth constituents, which may be on the order of tens of microns. Additionally, the optical mode overlap with the MQW may not be ideal in all sections due to the thickness variation. The relatively simple QWI process employed in this paper enables for the precise placement of the band edge of each component within the device, allowing for blue-shifted QWs to remain in the modulator while leaving the axial waveguide undisturbed.

For the first time, a widely tunable transmitter demonstrating negative chirp performance at 10 Gb/s over its entire tuning range has been fabricated. A simple, robust quantum-well-intermixing (QWI) processing platform was employed for the fabrication. The transmitter consists of a quantum-well electroabsorption modulator (QW-EAM) monolithically integrated with a widely tunable sampled grating (SG) distributed Bragg reflector (DBR) laser. Less than 0.5 dB power penalty was measured for transmission at 10 Gb/s through 75 km of standard fiber. Time resolved large signal chirp measurements demonstrated negative chirp characteristics over the 27–nm tuning range of the device in operating regimes providing over 10 dB of RF extinction and reasonable insertion loss. The QWI process avoids much of the complexity usually associated with the fabrication of laser/EAMs having negative chirp.

II. Background

A. QWI Integration Platform

This paper employs a modified ion-implantation enhanced QWI process described in [4], as the fabrication platform. In this process, vacancies are created by ion implantation into an InP buffer layer over the MQW active region. During a high temperature anneal, the vacancies are diffused through the MQW region, promoting the interdiffusion of group V-atoms between the wells and barriers. The interdiffusion reshapes the QW profile by distorting the QW/barrier interface. The result is a shift in the quantized energy levels in the well, and hence a shift in the band edge energy [4].

B. Device Architecture

The device architecture [Fig. 1(a)] consists of a five section widely tunable SG distributed Bragg reflector (DBR) laser followed by an EAM. The five sections of the SG-DBR laser are, from left to right in Fig. 1(a); backside absorber, rear mirror,

Manuscript received May 26, 2004; revised October 22, 2004. This work was supported by DARPA/MTO CS-WDM by Grant N66001-02-C-8026 and by Intel Corporation by Grant TXA001630000.

J. W. Raring and S. P. DenBaars are with the Materials Department, University of California, Santa Barbara, CA 93106 USA (e-mail: jraring@engineering.ucsb.edu).

E. J. Skogen, L. A. Johansson, M. N. Sysak, and L. A. Coldren are with the Electrical and Computer Engineering Department, University of California, Santa Barbara, CA 93106 USA.

Digital Object Identifier 10.1109/JLT.2004.840330

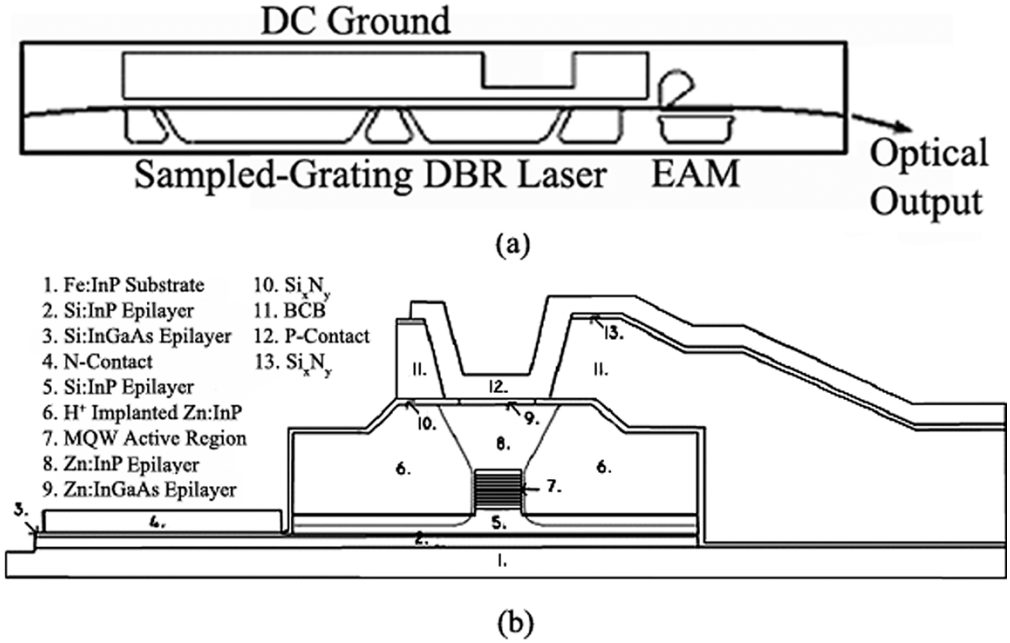

Fig. 1. (a) Top view schematic of the transmitter device architecture. (b) Cross-sectional schematic of modulator sections.

phase, gain, and front mirror. A buried ridge stripe waveguide design was employed with a curved/flared output to reduce the demands on the antireflection coating.

C. SG-DBR Laser

The SG DBR mirror is a special form of DBR mirror, where the gratings are periodically blanked to create a comb-like reflectivity spectrum [5]. The lithographically defined SG mirrors and the relatively simple process used to render the phase and mirror sections passive, make this device ideal for monolithic integration.

The sampling periods in the front and back mirrors differ, which provides the front and back mirrors with a different peak reflectivity spacing, so that only one set of reflectivity peaks is aligned within the desired tuning range. By differentially tuning the front and back mirrors a small amount, adjacent reflectivity peaks can be aligned, and the laser will operate at this new widely spaced wavelength. The simultaneous tuning of front and back mirrors allow wavelength coverage between mirror reflectivity peaks. The phase section provides cavity mode tuning, which ensures that the laser cavity mode is aligned with the mirror reflectivity peaks. The tuning in the mirrors and phase sections is based on carrier injection, producing a negative change in refractive index. To keep the loss to a minimal level over the desired wavelength operating range, the tuning sections make use of higher bandgap material or MQW regions whose quantized energy state is greater than that of the active region.

D. Electroabsorption Modulator

In an EAM, a reverse bias is used to shift the band edge of the modulator section to lower energy, thereby increasing the absorption of that region. In our case, QWI only smears the interfaces between the quantum wells and barriers, such that the quantum wells still remain after the intermixing, although slightly shallower and rounded. Allowing QWs to remain in the EAM enables the exploitation of the quantum-confined Stark effect in the EAM. The rounded shape of the intermixed quantum well also contributes to increased absorption efficiency in the modulator [6].

In this paper, several design and processing measures were taken to reduce parasitic capacitance in the EAM regions to achieve 10 Gb/s operation. The epilayer base structure was grown on a semiinsulating substrate. A 3-μm-thick layer of benzocyclobutene (BCB) was defined below the EAM bond pads to serve as a low-K dielectric. An angled proton implantation described in [7] was performed adjacent to the buried ridge to eliminate the parasitic capacitance associated with the homojunction. The implant was designed such that proton concentration was maintained at a level greater than 2E19 cm^{-2} to a depth beyond the InP homojunction on either side of the buried ridge. Fig. 1(b) is a schematic cross-sectional view of the EAM, illustrating these described features.

III. Process

The epitaxial base structure contained an n-contact InGaAs layer 1 μm below a multiquantum well (MQW) active region centered within a 1.1Q waveguide. The MQW consists of 15 InGaAsP 8.0 nm compressively strained (0.6%) quantum wells, separated by 8.0 nm tensile strained (0.3%) InGaAsP barriers grown on an Fe-doped InP substrate using a Thomas Swan horizontal-flow rotating-disk MOCVD reactor. Following the active region, a 15 nm InP stop etch, a 20-nm 1.3Q stop etch, and a 450-nm InP implant buffer layer was grown.

A 500-nm $\mathrm{Si}_x\mathrm{N}_y$, mask layer was deposited using plasma-enhanced chemical vapor deposition and lithographically patterned such that it remained over only the active regions of the chip. Next, ion implantation was performed using P^+ at an energy of 100 keV, yielding a range of 90 nm, with a dose of 5E14

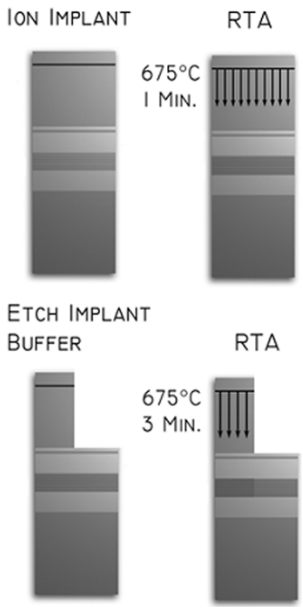

Fig. 2. Schematic of the intermixing process. From left to right on top; ion implantation followed by rapid thermal annealing. From left to right on bottom; selective removal of vacancy point defects required for blue-shifting, followed by an additional anneal.

cm^{-2}, at a substrate temperature of 200 °C [4]. The point defects created during the P^{+} implant were then partially diffused through the structure during a 60-s, 675 °C rapid thermal anneal (RTA), yielding the desired, 1510-nm photoluminescence band edge for the EAM. The implant buffer layer above the EAM sections was removed using a wet etching process, stopping on the 1.3Q stop etch layer. The sample was then subjected to an additional 180-s rapid thermal anneal, further blue-shifting the regions where the implant buffer layer remained. This second anneal was used to obtain desired band edge of 1450 nm for the mirror and phase sections. A schematic illustrating the intermixing process and the photoluminescence of the active, EAM, and passive regions are shown in Figs. 2 and 3, respectively.

The remainder of the process was carried out as described in [4] with the modifications for top-side n-contacts and the addition of BCB beneath the EAM contacts. The wafers were thinned, the devices were cleaved into bars and antireflection coated. The die were separated, soldered to aluminum nitride carriers, and wire bonded for characterization. A scanning electron micrograph of a completed devices mounted on a carrier is shown in Fig. 4.

IV. Device Results

The SG-DBR lasers demonstrated low threshold currents of 13 mA, with output powers of 10 mW captured in an integrating sphere at a gain section current of 100 mA as shown in Fig. 5. At this operating point, a side mode suppression ratio (SMSR) greater than 35 dB was achieved. By placing the MQW region in between a symmetrical waveguide maximum modal overlap is achieved, increasing the confinement factor by 50% over the traditional SG-DBR laser offset QW architecture [8].

The EAM 175 μm demonstrated over 40 dB of dc extinction for wavelengths of 1558, 1570, and 1580 nm, with efficiencies

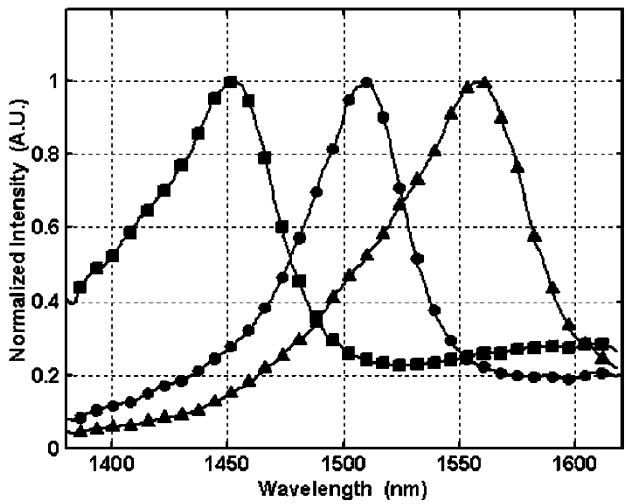

Fig. 3. Photoluminescence spectra of active section (triangles), modulator section (circles), and passive sections (squares).

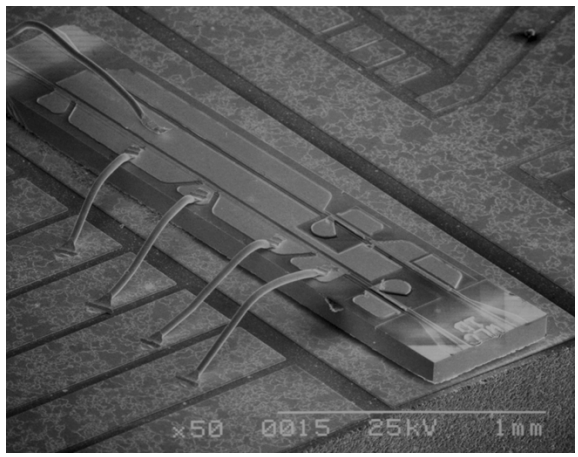

Fig. 4. Electron micrograph of transmitter device.

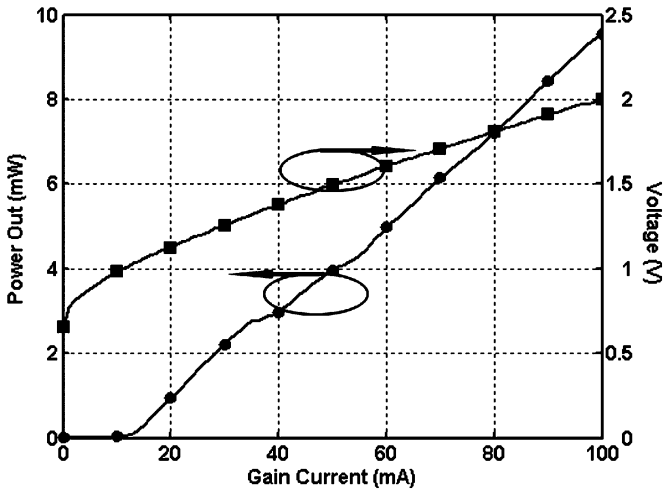

Fig. 5. Power out and gain section voltage versus applied current to SG-DBR laser gain section.

greater than 20 dB/V as shown in Fig. 6. The insertion loss of this EAM was found to be 1–2 dB at a wavelength of 1575 nm. The efficient extinction properties are due to the combination of the centered QW design and the intermixing process that allows

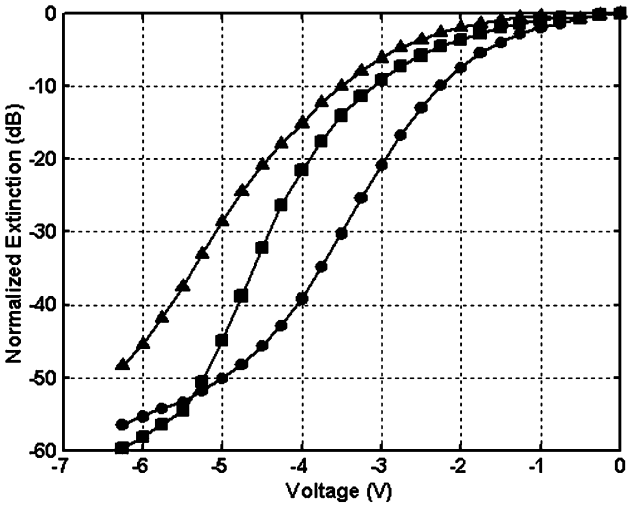

Fig. 6. DC extinction of a 175 μm modulator for wavelengths of 1558 nm (circles), 1570 nm (squares), and 1580 nm (triangles).

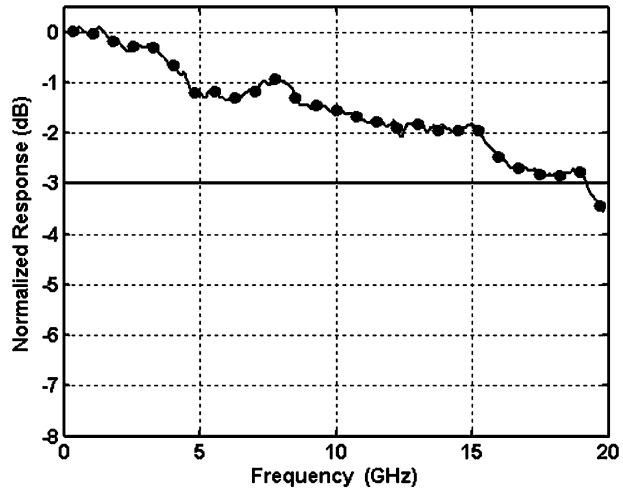

Fig. 7. Electrical to optical frequency response of a 175-μm modulator. The circular markers represent every 30th data point.

for precise placement of the modulator band edge. The 3-dB bandwidth, shown in Fig. 7, of the same modulator was greater than 19 GHz.

To demonstrate operation and transmission at 10 Gb/s, eye-diagrams were taken and bit-error rate (BER) testing was performed through various fiber lengths for the SG-DBR/EAM transmitters. The device was placed on a gold plated copper stage and cooled to 17 °C by a thermoelectric cooler. Light was coupled from the output facet of the transmitter device into a conical-tipped lensed fiber. The EAM was terminated with a 50-ohm resistor mounted directly on the ground-signal probes such that it was in parallel with the diode. A capacitor was placed in series with the termination resistor to eliminate dc power dissipation. The direct probing scheme was used to avoid the parasitics associated with the carrier and/or wire bonding. Back to back eye diagrams at 10 Gb/s were taken over the tuning range of the SG-DBR laser demonstrating RF extinction ratios greater than 10 dB using a dc driving voltage between 2.4 and 3.4 V with a 2.2-V peak to peak swing. The test setup and eye diagrams are shown in Figs. 8 and 9, respectively.

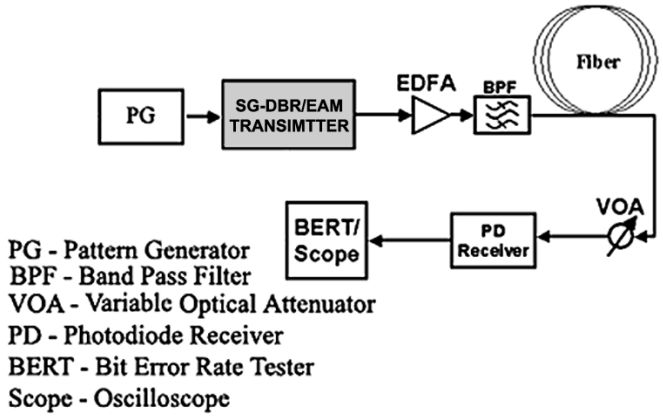

Fig. 8. Test set used to obtain BER and eye-diagrams from transmitter.

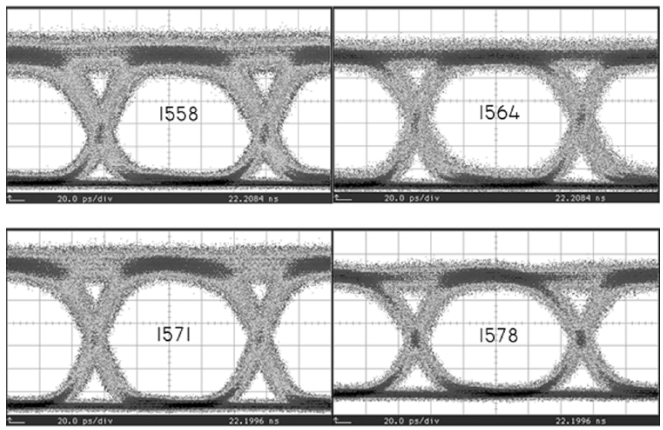

Fig. 9. Back-to-back eye diagrams from transmitter at wavelengths of 1558, 1564, 1571, and 1578 nm.

Transmission experiments at 10 Gb/s were performed using a nonreturn-to-zero (NRZ) pseudorandom-bit-sequence (PRBS) of $2^{31}-1$. A booster erbium doped fiber amplifier (EDFA) was used to launch optical powers on the order of 30 mW through Corning SMF-28 fiber. A variable optical attenuator was used to regulate the optical power into a nonpreamplified receiver. The complete test setup is shown in Fig. 8. Bit error rate (BER) curves through 25, 50, and 75 km of fiber at a wavelength of 1564 nm are shown in Fig. 4(b). Error-free operation was achieved through 75 km of fiber with a power penalty of less than 0.5 dB. The shaping of the eye diagrams due to dispersion is clearly seen in the insets of Fig. 10 where the optical eye diagrams are shown after transmission through fiber. The noise performance for transmission through 75 km is limited by the signal attenuation of the fiber and the noise of the oscilloscope optical receiver.

The low dispersion penalty for 10 Gb/s transmission demonstrated in Fig. 10 is indicative of negative chirp characteristics. For confirmation, the small-signal chirp parameter of the same device was extracted using the fiber-response method described in [9] for various EAM bias points at 1563 nm, as shown in Fig. 11. As expected, the EAM did exhibit negative chirp characteristics, with the transition from a positive to a negative chirp parameter occurring at -3.5 V

To demonstrate the capability for efficient 10 Gb/s transmission across the wide tuning range of these transmitters, the large

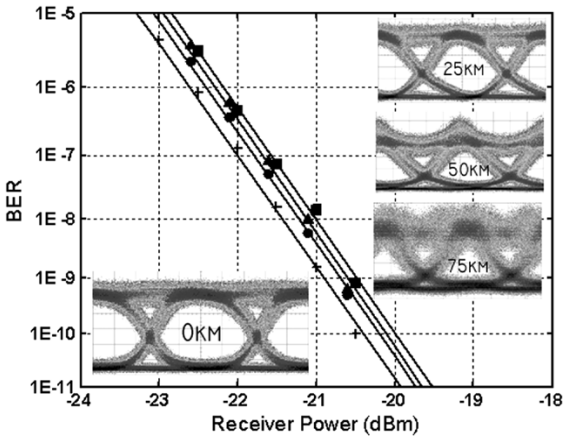

Fig. 10. BER curves and respective eye diagrams for back-to-back (cross), and transmission through 25 km (circles), 50 km (triangles), and 75 km (squares) of fiber at a wavelength of 1564 nm.

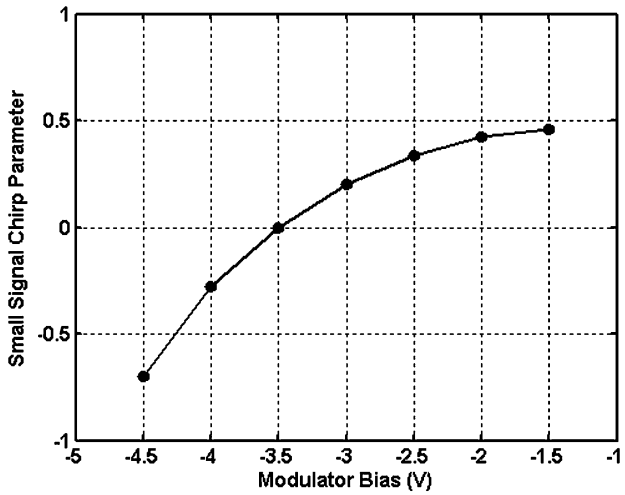

Fig. 11. The small signal chirp parameter characteristics versus reverse bias at 1563 nm.

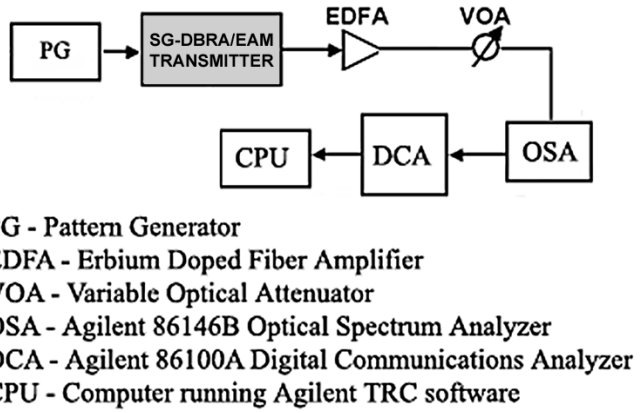

Fig. 12. Test setup used to extract time resolved large signal chirp parameter.

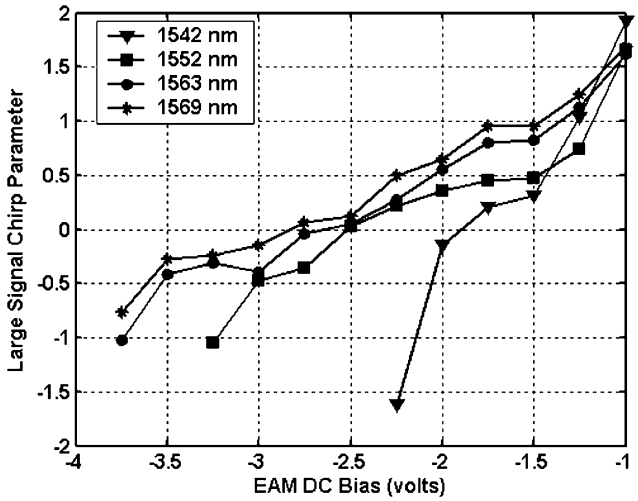

Fig. 13. Large signal chirp parameter as a function of EAM bias at 1542, 1552, 1562, and 1569 nm.

signal chirp parameter was extracted on a separate device at various wavelengths across its 27-nm tuning range. The large signal measurement is a better determination of the chirp characteristics of EAMs because it accounts for the full dynamic operating range essential for efficient transmission. That is the measurements can be made with an ac voltage swing necessary for > 10 dB signal extinction.

Large signal chirp measurements were made using Agilent's Time Resolved Chirp (TRC) software coupled with the required Agilent 86 146B optical spectrum analyzer and 86 100 A digital communications analyzer. The complete test setup is illustrated in Fig. 12. The chirp parameter was measured as a function of the dc bias applied to the EAM for wavelengths of 1542, 1552, 1562, and 1569 nm. The laser gain section was biased at 50 mA with the appropriate mirror section currents to achieve each wavelength while the peak-to-peak voltage swing applied to the EAM was 2 V. As shown in Fig. 13, a larger reverse bias is required to achieve a negative chirp parameter at longer wavelengths. The measured chirp parameters were found to transition from positive to negative for all wavelengths, occurring at 1.9 V at 1542 nm and 2.8 V at 1569 nm.

Considering the proximity of the modulator band edge to the laser operating wavelength, it is clear that a larger reverse bias is required to achieve efficient absorption at longer wavelengths. The onset of absorption with reverse voltage increases and the absorption efficiency decreases somewhat with increasing wavelength, however, the general shape of the extinction curves remain similar. In view of the fact that the chirp parameter is related to the operating point on the modulator extinction curve, and the fact that similar extinction characteristics are observed for all wavelengths, our demonstration of a negative chirp parameter over the wide tuning range of the SG-DBR laser is perfectly reasonable.

To demonstrate that the negative chirp characteristics of the transmitter can be achieved within an operating regime providing sufficient signal extinction and reasonable output power across its tuning range, the modal extinction characteristics were evaluated with respect to the large signal chirp data at each wavelength. By comparing the extinction characteristics in Fig. 14 with the chirp characteristics of the same device in Fig. 13, the modulator extinction ratio and insertion loss can be estimated for a given chirp parameter at all tested wavelengths. The intersections of the dashed and dotted lines on in Fig. 14 represent the on-state operating voltage of the EAM to achieve

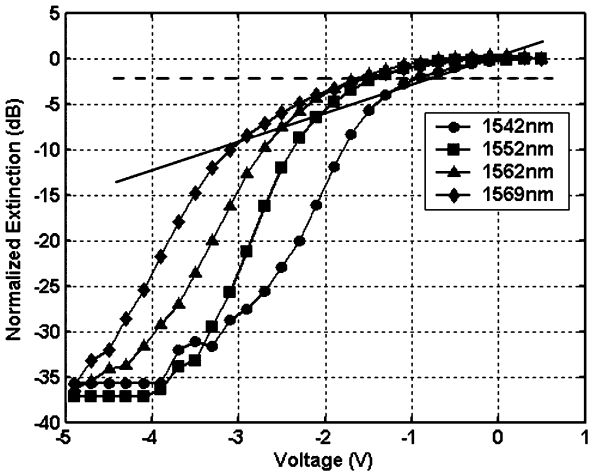

Fig. 14. DC extinction of the 175 μm modulator for wavelengths from 1542 to 1569 nm from the same modulator in which the large signal chirp was extracted from. The dashed and solid lines indicate the approximate EAM on state dc bias to achieve a chirp parameter of 0 and -0.7, respectively, with a 2 V peak to peak swing.

chirp parameters of 0 and -0.7, respectively. The on-state operating voltage was calculated by adding 1/2 of the peak to peak voltage swing (1 V) to the dc bias necessary to achieve the chirp parameter values in question. It is clear that for both chirp parameter values, a 2-V swing on the EAM provides over 10 dB extinction at all tested wavelengths. Fig. 14 indicates that to achieve a chirp parameter of 0, the modulator must be biased such that there is only $\sim$2 dB of on-state signal extinction for all tested wavelengths. To achieve a chirp parameter of -0.7, the on-state signal extinction ranged from 3.5 dB at 1542 nm to 9 dB at 1569 nm. With these extinction values, the total insertion loss of the EAM can be estimated at each wavelength for operation at both chirp parameter values by adding the unbiased insertion loss, which we have extracted to be 1-2 dB at 1575 nm. Although the unbiased insertion loss will increase with decreasing operation wavelength, the signal extinction required for negative chirp is decreased with decreasing wavelength. The key point is that to achieve chirp parameter values necessary for low penalty 10 Gb/s transmission the EAMs are not forced to operate at a bias point along the extinction curve which provides unacceptable insertion loss or insufficient extinction.

V. Conclusion

For the first time, we have realized a high performance widely tunable laser/EAM transmitter capable of negative chirp operation across its entire tuning range. The transmitter demonstrated error-free low-power-penalty operation through 75 km of standard fiber at 10 Gb/s. The large signal chirp parameter was shown to transition to a negative value at larger reverse biases for increasing operation wavelength. Furthermore, it was shown that the operation regime required for negative chirp characteristics provided sufficient signal extinction and reasonable insertion loss. The 3-dB bandwidth of this transmitter was shown to be over 19 GHz with an RF extinction greater than 10 dB. This work was made possible by the use of a simple, robust QWI processing platform for the monolithic integration of blue-shifted QW-EAMs with SG-DBR lasers.

References

[1] Y. Akulova, G. Fish, P. Koh, C. Schow, P. Kozodoy, A. Dahl, S. Nakagawa, M. Larson, M. Mack, T. Strand, C. Coldren, E. Hegblom, S. Penniman, T. Wipiejewski, and L. Coldren, "Widely tunable electroabsorption-modulated sampled grating DBR laser transmitter," *IEEE J. Sel. Topics Quantum Electron.*, vol. 8, pp. 1349–1357, Nov./Dec. 2002.

[2] K. Morito, R. Sahara, K. Sato, and Y. Kotaki, "Penalty free 10 Gb/s NRZ transmission over 100 km of standard fiber at 1.55 μm with a blue-chirp modulator integrated DFB laser," *IEEE Photon. Technol. Lett.*, vol. 8, pp. 431–433, 1996.

[3] J. Binsma, P. Thijs, T. VanDongen, E. Jansen, A. Staring, G. VanDenHoven, and L. Tiemeijer, "Characterization of butt-joint InGaAsP waveguides and their application to 1310 nm DBR-type MQW ganin-clamped semiconductor optical amplifiers," *IEICE Trans. Electron.*, vol. E80-C, pp. 675–681, 1997.

[4] E. Skogen, J. Raring, J. Barton, S. DenBaars, and L. Coldren, "Post-growth control of the quantum well band edge for the monolithic integration of widely tunable lasers and electroabsorption modulators," IEEE J. Sel. Topics Quantum Electron., 2004, to be published.

[5] V. Jayaraman, Z. Chuang, and L. Coldren, "Theory, design, and performance of extended tuning range semiconductor lasers with sampled gratings," *IEEE J. Quantum Electron.*, vol. 29, pp. 1824–1834, 1993.

[6] S. Charbonneau, E. Kotels, P. Poole, J. He, G. Aers, J. Haysom, M. Buchanan, Y. Feng, A. Delage, F. Yang, M. Davies, R. Goldberg, P. Piva, and I. Mitchell, "Photonic integrated circuits fabricated using ion implantation," *IEEE J. Sel. Topics Quantum Electron.*, vol. 4, pp. 772–793, 1998.

[7] J. Raring, E. Skogen, L. Johansson, and L. Coldren, "Enhanced frequency response in buried ridge quantum well intermixed SGDBR laser modulators," in *Conf. Lasers Electro-Optics*, San Francisco, CA, May 16–21, 2004.

[8] B. Mason, J. Barton, G. Fish, and L. Coldren, "Design of sampled grating DBR lasers with integrated semiconductor optical amplifiers," *IEEE Photon. Technol. Lett.*, vol. 12, pp. 762–764, 2000.

[9] B. Dvaux, Y. Sorel, and J. F. Kerdiles, "Simple measurement of fiber dispersion and of chirp parameter of intensity modulated light emitter," *J. Lightw. Technol.*, vol. 11, no. 12, pp. 1937–1940, Dec. 1993.

James W. Raring (S'03) was born in Ramsey, NJ, in 1978. He received the B.S. degree from the Materials Engineering Department, California Polytechnic State University, San Luis Obispo, in 2001.

He is currently pursuing the Ph.D. degree in materials science from the University of California, Santa Barbara. His current research focuses on the monolithic integration of widely tunable diode lasers into high-speed photonic integrated circuits with the use of quantum-well intermixing and MOCVD growth.

Erik J. Skogen (M'99) was born in Minneapolis, MN, in 1975. He received the B.S. degree from Iowa State University in 1997, and the M.S. and Ph.D. degrees from the University of California, Santa Barbara, in 1999 and 2003, respectively.

His current research interests include widely tunable semiconductor lasers, monolithic integration for photonic integrated circuits, growth aspects in the InGaAsP material system using MOCVD, and quantum-well intermixing.

Leif A. Johanasson (M'04) received the Ph.D. degree in engineering from University College London in 2002.

He continued with a Postdoctoral position with the University of California, Santa Barbara, in 2002. His current research interests include design and characterization of integrated photonic devices for analog and digital applications.

Mathew N. Sysak (M'03) was born in Smithtown, NY, in 1976. He received the B.S. degree from Pennsylvania State University in chemical engineering in 1998 and the M.S. degree from the University of California, Santa Barbara, in electrical and computer engineering.

His current research interests include the monolithic integration of widely tunable semiconductor lasers with semiconductor optical amplifiers, electroabsorption modulators, and photodetectors in the InGaAsP material system.

Steven P. DenBaars (M'91) from 1988 to 1991, he was a member of Technical Staff at Hewlett-Packard where he was involved in the fabrication of high brightness LEDs. In 1991 he joined the faculty of the University of California, Santa Barbara (UCSB), as a Professor of materials and electrical engineering, where he is developing new solid-state optoelectronic devices. His research also involves MOCVD growth of GaN- and InP-based tunable lasers and detectors. Currently, he is an Associate Director of the solid-state lighting and display center (SSLDC) at UCSB, which is developing new more-energy efficient light sources. Special interests include the effect of materials properties on device performance, blue VCSEL lasers, and microwave power transistors. He has authored more than 200 technical publications, three book chapters, 100 conference presentations, and more than seven patents.

Dr. DenBaars has received a NSF Young Scientist Award (1995) and the Young Scientist Award from the International Symposium on Compound Semiconductors in 1998.

Larry A. Coldren (F'80) received the Ph.D. degree in electrical engineering from Stanford University, Stanford, CA, in 1972.

He is the Fred Kavli Professor of Optoelectronics and Sensors at the University of California (UCSB), Santa Barbara. He is also Chairman and Chief Technology Officer of Agility Communications, Inc. After 13 years in the research area at Bell Laboratories, he joined UCSB in 1984 where he now holds appointments in Materials and Electrical and Computer Engineering, and is Director of the Optoelectronics Technology Center. In 1990 he cofounded Optical Concepts, later acquired as Gore Photonics, to develop novel VCSEL technology; and in 1998 he cofounded Agility Communications to develop widely tunable integrated transmitters. At Bell Labs, he initially worked on waveguided surface-acoustic-wave signal processing devices and coupled-resonator filters. He later developed tunable coupled-cavity lasers using novel reactive-ion etching (RIE) technology that he created for the then new InP-based materials. At UCSB he continued work on multiple-section tunable lasers, in 1988 inventing the widely tunable multielement mirror concept, which is now fundamental to many of Agility's products. During the late 1980s, he also developed efficient vertical-cavity multiple-quantum-well modulators, which led to novel vertical-cavity surface-emitting laser (VCSEL) designs that provided unparalleled levels of performance. He continues to be active in developing new photonic integrated circuit (PIC) and VCSEL technology, including the underlying materials growth and fabrication techniques. In recent years, for example, he has been involved in the creation of vertical and in-plane GaN-based emitters, efficient all-epitaxial InP-based VCSELs, and a variety of PICs incorporating numerous optical elements for widely tunable integrated transmitters, receivers, and wavelength converters. He has authored or coauthored more than 700 papers, five book chapters, one textbook, and has been issued 36 patents.

Professor Coldren has presented dozens of invited and plenary talks at major conferences. He is a fellow of the OSA and IEE, the recipient of the 2004 John Tyndall Award, and a member of the National Academy of Engineering.